ESTIMATING THE AVERAGE SIZE OF FIBER/MATRIX INTERFACE CRACKS IN UD AND CROSS-PLY LAMINATES

L. Di Stasio[1,2], J. Varna[1], Z. Ayadi[2]

[1]Division of Materials Science, Luleå University of Technology, Luleå, Sweden
[2]EEIGM & IJL, Université de Lorraine, Nancy, France

7th ECCOMAS Thematic Conference on the Mechanical Response of Composites
Girona (ES) - September 18-20, 2019

Outline

TRANSVERSE CRACKS INITIATION IN FRPC

Micromechanics of Initiation: Transverse Tensile Loading

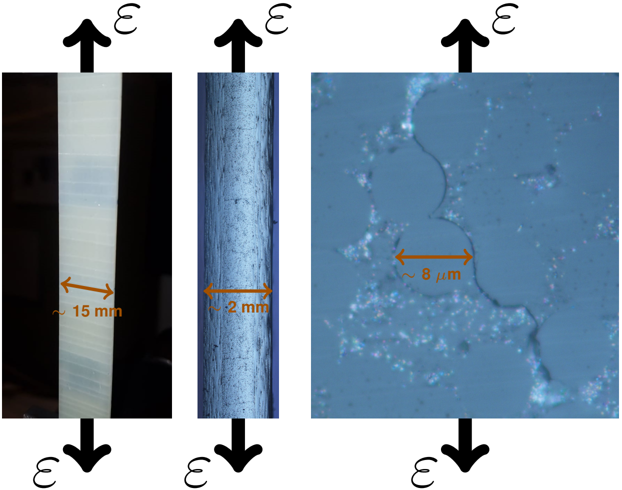

Left:
front view of $[0, 90_2]_S$, visual inspection.

Center:
edge view of $[0, 90]_S$, optical microscope.

Right:
edge view of $[0, 90]_S$, optical microscope.

Micromechanics of Initiation: Transverse Tensile Loading

Stage 1: isolated debonds

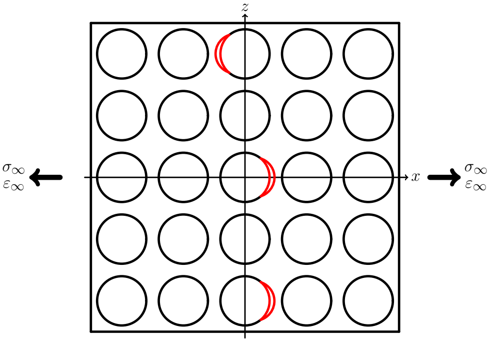

Bailey et al., P. Roy. Soc. A-Math. Phy. **366** (1727), 1979.

Bailey et al., J. Mater. Sci. **16** (3), 1981.

Zhang et al., Compos. Part A-Appl. S. **28** (4), 1997.

Micromechanics of Initiation: Transverse Tensile Loading

Stage 2: consecutive debonds

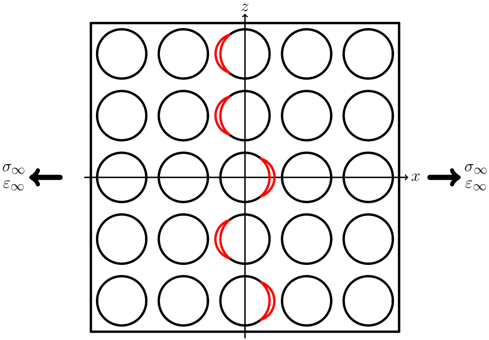

Bailey et al., P. Roy. Soc. A-Math. Phy. **366** (1727), 1979.

Bailey et al., J. Mater. Sci. **16** (3), 1981.

Zhang et al., Compos. Part A-Appl. S. **28** (4), 1997.

Micromechanics of Initiation: Transverse Tensile Loading

Stage 3: kinking

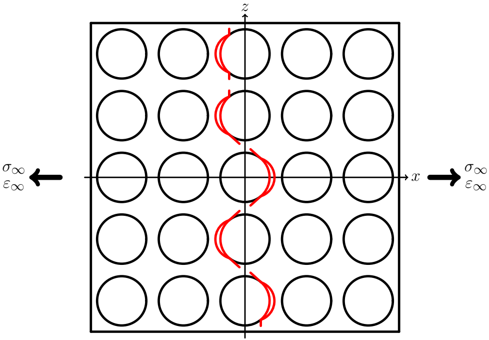

Bailey et al., P. Roy. Soc. A-Math. Phy. **366** (1727), 1979.

Bailey et al., J. Mater. Sci. **16** (3), 1981.

Zhang et al., Compos. Part A-Appl. S. **28** (4), 1997.

Micromechanics of Initiation: Transverse Tensile Loading

Stage 4: coalescence

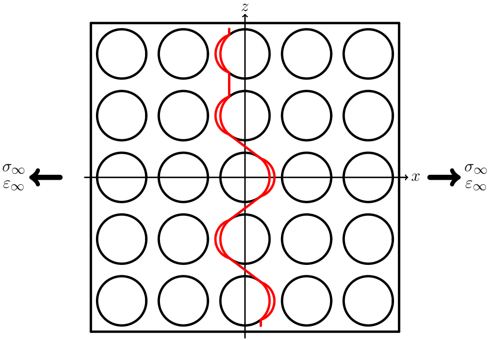

Bailey et al., P. Roy. Soc. A-Math. Phy. **366** (1727), 1979.

Bailey et al., J. Mater. Sci. **16** (3), 1981.

Zhang et al., Compos. Part A-Appl. S. **28** (4), 1997.

Objective of the Study

Can we talk about a ply-thickness effect for the fiber-matrix interface crack?

Stage 1: isolated debonds

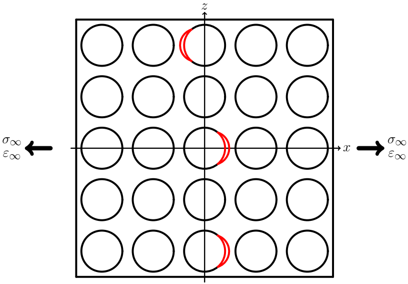

Stage 2: consecutive debonds

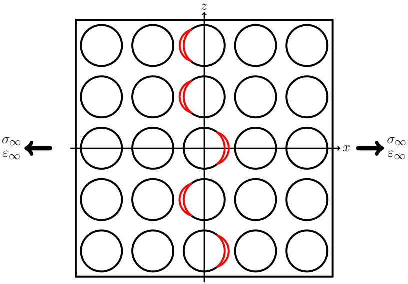

↘ Modeling

Geometry

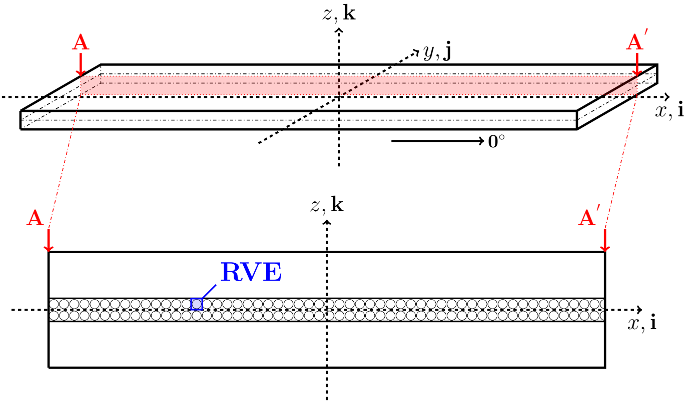

- ➔ $L, W >> t$
- ➔ $L, W \to \infty$
- ➔ Square packing
- ➔ $L_d >> \Delta\theta_d$
- ➔ 2D RVE

Representative Volume Elements

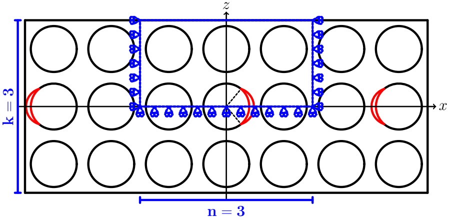

$n \times k - free$

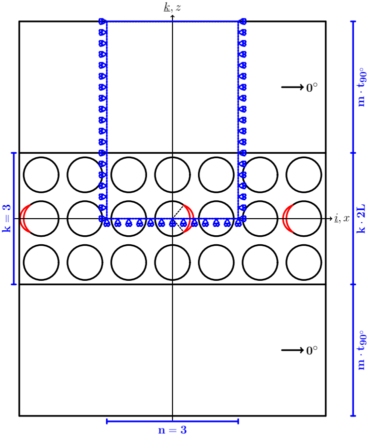

$n \times k - m \cdot t_{90^\circ}$

Representative Volume Elements

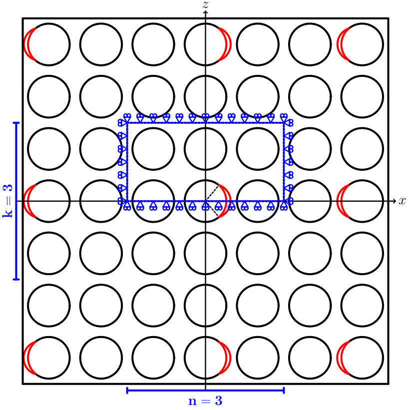

$n \times k - symm$

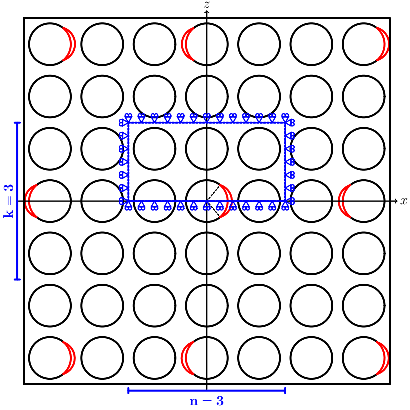

$n \times k - asymm$

Assumptions

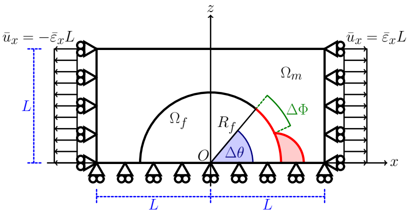

$R_f = 1 \;\; [\mu m] \qquad L = \frac{R_f}{2}\sqrt{\frac{\pi}{V_f}}$

- ➔ Linear elastic, homogeneous materials
- ➔ Concentric Cylinders Assembly with Self-Consistent Shear Model for UD
- ➔ Plane strain
- ➔ Frictionless contact interaction
- ➔ Symmetric w.r.t. x-axis
- ➔ Coupling of x-displacements on left and right side (repeating unit cell)
- ➔ Applied uniaxial tensile strain $\bar{\varepsilon}_x = 1\%$
- ➔ $V_f = 60\%$

Material	V_f [%]	E_L [GPa]	E_T [GPa]	μ_{LT} [GPa]	ν_{LT} [$-$]	ν_{TT} [$-$]
Glass fiber	-	70.0	70.0	29.2	0.2	0.2
Epoxy	-	3.5	3.5	1.25	0.4	0.4
UD	60.0	43.442	13.714	4.315	0.273	0.465

Solution

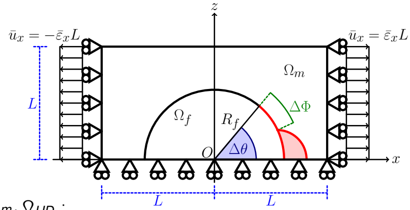

in $\Omega_f, \Omega_m, \Omega_{UD}$:

$$\frac{\partial^2 \varepsilon_{xx}}{\partial z^2} + \frac{\partial^2 \varepsilon_{zz}}{\partial x^2} = \frac{\partial^2 \gamma_{zx}}{\partial x \partial z}$$

$$\varepsilon_y = \gamma_{xy} = \gamma_{yz} = 0$$

$$\frac{\partial \sigma_{xx}}{\partial x} + \frac{\partial \tau_{zx}}{\partial z} = 0$$

$$\frac{\partial \tau_{zx}}{\partial x} + \frac{\partial \sigma_{zz}}{\partial z} = 0$$

$$\sigma_{yy} = \nu \left(\sigma_{xx} + \sigma_{zz}\right)$$

for $0^\circ \leq \alpha \leq \Delta\theta, \Delta\theta \neq 0^\circ$:

$$\left(\vec{u}_m\left(R_f, \alpha\right) - \vec{u}_f\left(R_f, \alpha\right)\right) \cdot \vec{n}_\alpha \geq 0$$

for $\Delta\theta \leq \alpha \leq 180^\circ$:

$$\vec{u}_m\left(R_f, \alpha\right) - \vec{u}_f\left(R_f, \alpha\right) = 0$$

$$\sigma_{ij} = E_{ijkl}\varepsilon_{kl}$$

$$+ BC$$

$\forall\ \Delta\theta \neq 0^\circ$

→ oscillating singularity

$$\sigma \sim r^{-\frac{1}{2}} \sin\left(\varepsilon \log r\right), \quad V_f \rightarrow 0$$

$$\varepsilon = \frac{1}{2\pi} \log\left(\frac{1-\beta}{1+\beta}\right)$$

$$\beta = \frac{\mu_2\left(\kappa_1 - 1\right) - \mu_1\left(\kappa_2 - 1\right)}{\mu_2\left(\kappa_1 + 1\right) + \mu_1\left(\kappa_2 + 1\right)}$$

→ receding contact

→ $\dfrac{G\left(R_{f,2}\right)}{G\left(R_{f,1}\right)} = \dfrac{R_{f,2}}{R_{f,1}}, \quad \dfrac{G\left(\bar{\varepsilon}_{x,2}\right)}{G\left(\bar{\varepsilon}_{x,1}\right)} = \dfrac{\bar{\varepsilon}^2_{x,2}}{\bar{\varepsilon}^2_{x,1}}$

→ FEM + LEFM (VCCT)

→ regular mesh of quadrilaterals at the crack tip:

- $AR \sim 1, \quad \delta = 0.05^\circ$

$\forall\ \Delta\theta$

→ 2^{nd} order shape functions

↘ DEBOND INITIATION

σ_{rr} vs $\tau_{r\theta}$: radial stress vs tangential shear at the interface

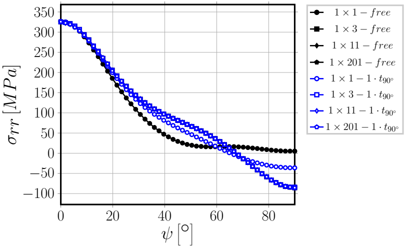

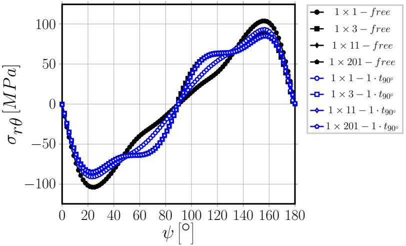

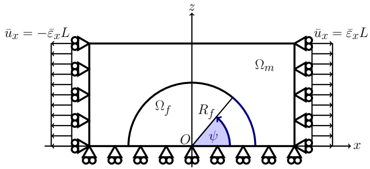

σ_{rr} vs $\tau_{r\theta}$: radial stress vs tangential shear at the interface

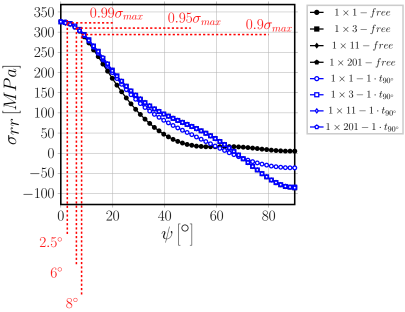

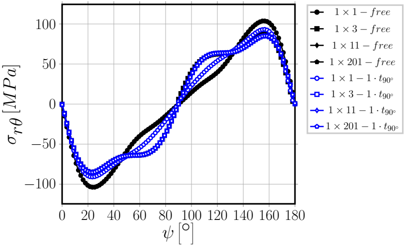

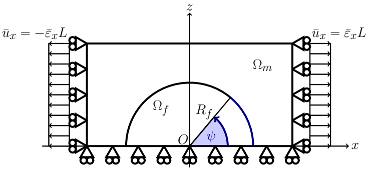

σ_{LHS}: local hydrostatic stress at the interface

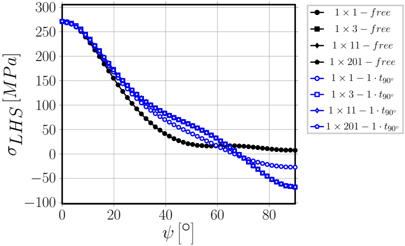

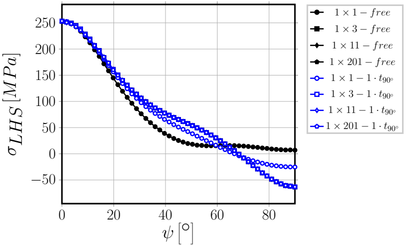

$$\sigma^{2D}_{LHS} = \frac{\sigma_{rr} + \sigma_{\theta\theta}}{2}$$

$$\sigma^{3D}_{LHS} = \frac{\sigma_{rr} + \sigma_{\theta\theta} + \sigma_{yy}}{3}$$

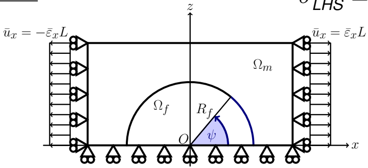

σ_{LHS}: local hydrostatic stress at the interface

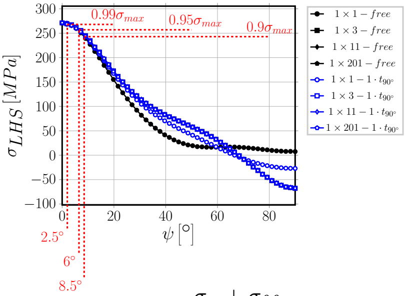

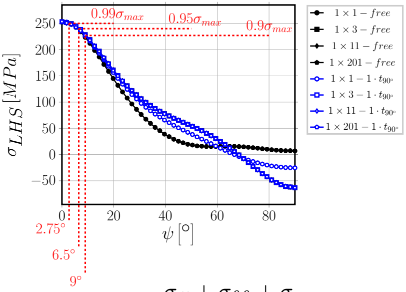

$$\sigma_{LHS}^{2D} = \frac{\sigma_{rr} + \sigma_{\theta\theta}}{2}$$

$$\sigma_{LHS}^{3D} = \frac{\sigma_{rr} + \sigma_{\theta\theta} + \sigma_{yy}}{3}$$

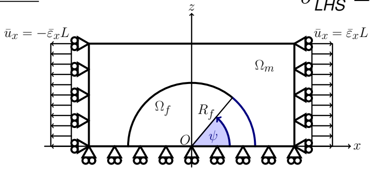

$\sigma_{\mathbf{vM}}$: von Mises stress at the interface

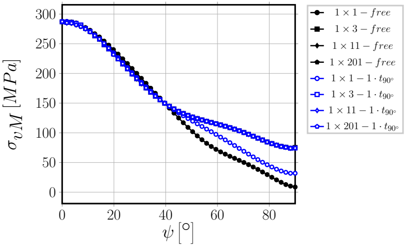

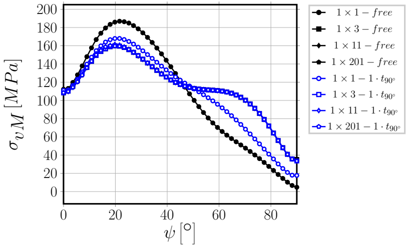

$$\sigma_{vM}^{2D} = \sqrt{(\sigma_{rr} - \sigma_{\theta\theta})^2 + 3\tau_{12}^2}$$

$$\sigma_{LHS}^{3D} = \frac{3}{2} s_{ij} s_{ij} \quad s_{ij} = \sigma_{ij} - \frac{1}{3}\sigma_{kk}\delta_{ij}$$

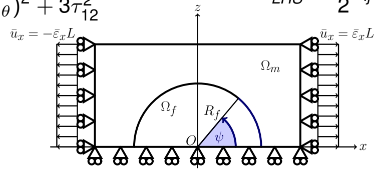

σ_{vM}: von Mises stress at the interface

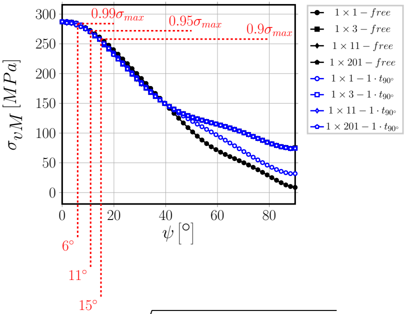

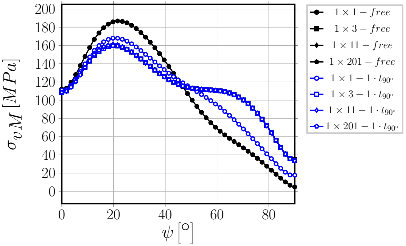

$$\sigma_{vM}^{2D} = \sqrt{(\sigma_{rr} - \sigma_{\theta\theta})^2 + 3\tau_{12}^2}$$

$$\sigma_{LHS}^{3D} = \frac{3}{2} s_{ij} s_{ij} \quad s_{ij} = \sigma_{ij} - \frac{1}{3}\sigma_{kk}\delta_{ij}$$

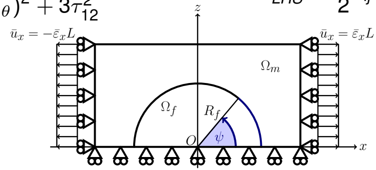

σ_{I}: maximum principal stress at the interface

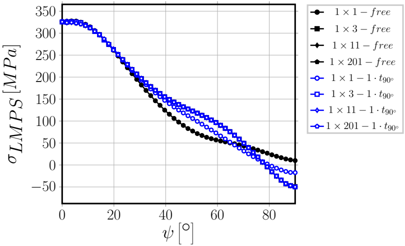

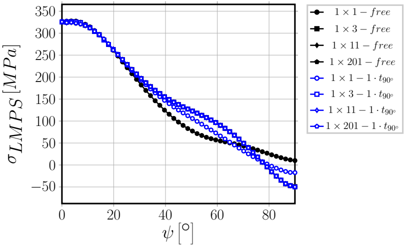

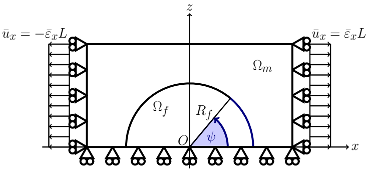

σ_{I}: maximum principal stress at the interface

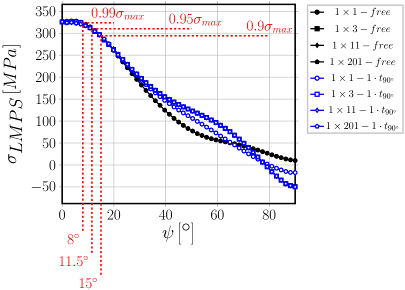

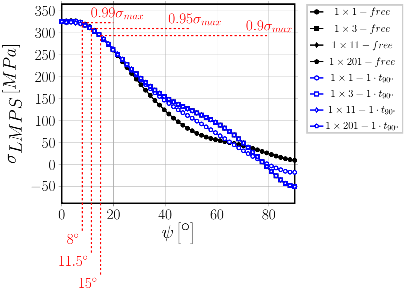

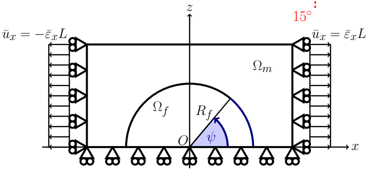

Observations & Conclusions

- ➔ For all stresses analyzed, no significant difference is present between the different RUCs for $\psi \leq 10^{\circ}$;
- ➔ for all stresses analyzed, no difference can be observed by increasing k when $k \geq 3$;
- ➔ for all stresses analyzed, no difference can be observed between $1 \times k - free$ and $1 \times k - 1 \cdot t_{90^{\circ}}$ for $k \geq 3$;
- ➔ σ_{rr}, $\sigma_{LHS,2D}$, $\sigma_{LHS,3D}$, $\sigma_{vM,2D}$, $\sigma_{LMPS,2D}$ and $\sigma_{LMPS,3D}$ all reach their peak value at 0° and 180° and decrease to 99% the peak value between 2° and 8°, to 95% the peak value between 6° and 12° and to 90% the peak value between 8° and 15° from the occurrence of the maximum.

It seems reasonable to conclude that...

...a stress-based criterion would predict, irrespectively of the specific criterion chosen, the onset of an interface crack at 0° or 180° with an initial size at least comprised in the range $2^{\circ} - 8^{\circ}$ (1% margin) and likely in the range $6^{\circ} - 12^{\circ}$ (5% margin).

↘ DEBOND PROPAGATION

Estimation of G_{Ic}

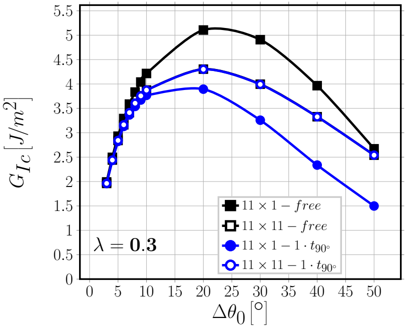

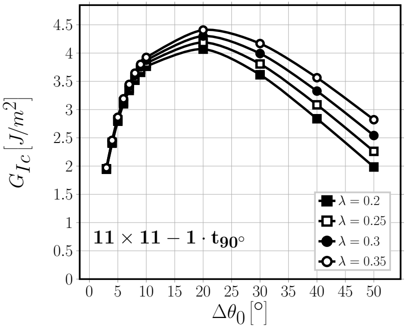

$$G_{Ic} = \left.\frac{G_c}{1 + \tan^2\left(\left(1 - \lambda\right)\Psi_G\right)}\right|_{G_c = G_{TOT}(\Delta\theta_0)}, \quad \Psi_G = \left. tan^{-1}\left(\sqrt{\frac{G_{II}}{G_I}}\right)\right|_{\Delta\theta_0}$$

Estimation of $\Delta\theta_{max}$

$21 \times 1 - free$

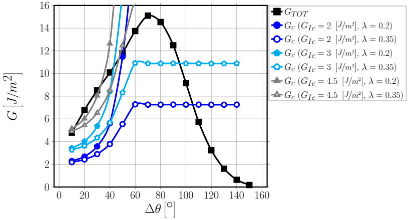

$\Delta\theta_{max} \in (30^\circ - 105^\circ)$

$21 \times 1 - 1 \cdot t_{90^\circ}$

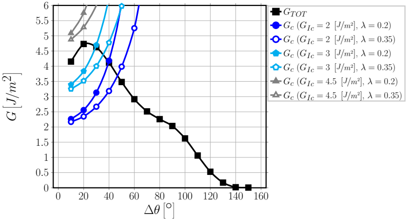

$\Delta\theta_{max} \in (30^\circ - 50^\circ)$

$$G_{TOT}(\Delta\theta) > G_c = G_{Ic}\left(1 + \tan^2\left(\left(1-\lambda\right)\Psi_G\right)\right), \quad \Psi_G = tan^{-1}\left(\sqrt{\frac{G_{II}}{G_I}}\right)\Bigg|_{\Delta\theta}$$

Estimation of $\Delta\theta_{max}$

$21 \times 3 - free$

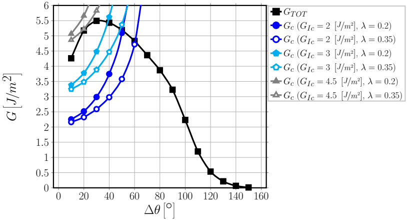

$\Delta\theta_{max} \in (40^\circ - 60^\circ)$

$21 \times 3 - 1 \cdot t_{90^\circ}$

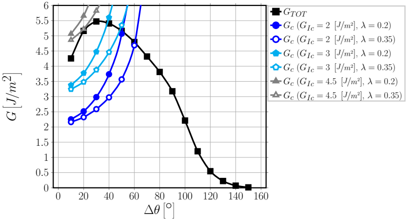

$\Delta\theta_{max} \in (40^\circ - 60^\circ)$

$$G_{TOT}(\Delta\theta) > G_c = G_{Ic}\left(1 + \tan^2\left((1-\lambda)\Psi_G\right)\right), \quad \Psi_G = tan^{-1}\left(\sqrt{\frac{G_{II}}{G_I}}\right)\Bigg|_{\Delta\theta}$$

Estimation of $\Delta\theta_{max}$

$21 \times 21 - free$

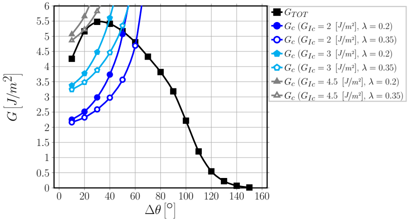

$\Delta\theta_{max} \in (40° - 60°)$

$21 \times 21 - 1 \cdot t_{90°}$

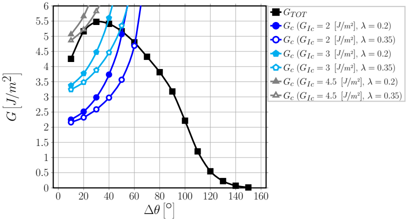

$\Delta\theta_{max} \in (40° - 60°)$

$$G_{TOT}(\Delta\theta) > G_c = G_{Ic}\left(1 + \tan^2\left((1-\lambda)\Psi_G\right)\right), \quad \Psi_G = tan^{-1}\left(\sqrt{\frac{G_{II}}{G_I}}\right)\Bigg|_{\Delta\theta}$$

Estimation of $\Delta\theta_{max}$

$21 \times 21 - symm$

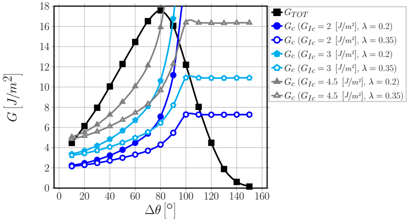

$\Delta\theta_{max} \in (80^\circ - 110^\circ)$

$21 \times 21 - asymm$

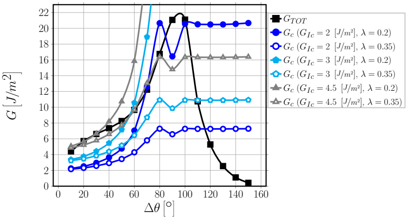

$\Delta\theta_{max} \in (55^\circ - 115^\circ)$

$$G_{TOT}(\Delta\theta) > G_c = G_{Ic}\left(1 + \tan^2\left(\left(1-\lambda\right)\Psi_G\right)\right), \quad \Psi_G = tan^{-1}\left(\sqrt{\frac{G_{II}}{G_I}}\right)\Bigg|_{\Delta\theta}$$

Observations & Conclusions

- ➔ The effect of the presence of the 0° layer is to reduce the maximum size of debonds;
- ➔ however, the estimated debond size is the same for $n \times k - free$ and $n \times k - 1 \cdot t_{90^{\circ}}$ for $k \geq 3$;
- ➔ the presence of a debond on the neighboring fiber in the vertical direction ($21 \times 1 - coupling$ and $21 \times 1 - asymm$) favors instead the growth of larger debonds;
- ➔ the largest size is achieved when debonds are on opposite sides of consecutive fibers.

Estimated debond size range in cross-ply ($n \times k - 1 \cdot t_{90^{\circ}}$)

$40^{\circ} - 60^{\circ}$

Measured debond size range in cross-ply (Correa et al., Compos. Sci. Technol. 155 (213-220), 2018**)**

$21.4^{\circ} - 89.2^{\circ}$, average 49.3°, standard deviation of 11.7°
63% of measurements in $40^{\circ} - 60^{\circ}$ range

Conclusions

Conclusions

- A stress criterion for initiation would likely predict, irrespectively of which criterion from those proposed in the literature is chosen, the onset of a debond at 0° or 180° with a semi-aperture $\Delta\theta_0$ in the range $2^{\circ} - 12^{\circ}$, corresponding to a margin of 5% on the satisfaction of the criterion.
- Assuming that debond propagation occurs unstably immediately after debond onset at the same level of global applied strain $\bar{\varepsilon}_x$, it is possible to evaluate the parameter G_{Ic} in the expression of the critical ERR and with it to estimate the range of expected maximum debond size.
- The prediction for a cross-ply laminate (models $n \times k - 1 \cdot t_{90^{\circ}}$, $k \geq 3$) agrees well with the debond size distribution in $\left[0^{\circ}_{3}, 90^{\circ}_{3}\right]_S$ estimated in *Correa et al., Compos. Sci. Technol.* ***155*** *(213-220), 2018* through microscopic observations.

Thank you for listening today!

DocMASE

UNIVERSITÉ DE LORRAINE

EEIGM

LULEÅ UNIVERSITY OF TECHNOLOGY

Education and Culture

Erasmus Mundus